Mechanical Fatigue of Thin Copper Foil

H.D. MERCHANT,[1] M.G. MINOR,[1] and Y.L. LIU[2]

1.—Gould Electronics, Eastlake, OH 44095-4001. 2.—University of Kentucky, Lexington, KY 40506-0046.

The electrodeposited and the rolled 12 to 35 μm thick copper foils are subjected to the bending/unbending strain-controlled flex fatigue over a wide range of strain amplitudes. The fatigue life is associated with an increase in electrical resistance of the specimen beyond a preassigned threshold. For each foil type, in the rolled or as-deposited as well as in the (recrystallization-like) annealed conditions, the inverse Coffin-Manson (C-M) relationship between strain amplitude ($\Delta\varepsilon/2$) and fatigue life (N_f) is established in the high $\Delta\varepsilon/2$ (low N_f) and the low $\Delta\varepsilon/2$ (high N_f) regimes. The N_f, $\Delta\varepsilon/2$, and C-M slopes (c,b) are utilized to calculate the cyclic strain hardening (n′) and fatigue ductility (D_f) parameters. It is shown that for a given foil thickness, an universal relationship exists between D_f and the strength (σ) normalized fatigue life (N_f/σ). The propagation of fatigue crack through the foil thickness and across the sample width is related to the unique fine grain structure for each foil type: pancaked grains for the rolled foil and equiaxed grains for the electrodeposited foil. The fatal failure corresponds to convergence of the through-thickness and the across-the-width fatigue cracks. The variations in (i) electrical resistance, (ii) mid-thickness microhardness and grain structure and (iii) dislocation configurations with fatigue are monitored. Except for a small but significant fatigue induced softening (or hardening), no convincing evidence of strain localization (and the associated dislocation configurations generally observed for the bulk samples) has been found.

Key words: Copper foil, mechanical fatigue, Coffin-Manson relationship, electrodeposited

INTRODUCTION

Several uniaxial tension/tension mode stress-controlled fatigue studies for the thin rolled[1] as well as electrodeposited[2] copper foil have been reported. The uniaxial tension/compression mode fatigue characterization of the thin foil is made possible by utilizing a vibration exciter (<50,000 H_z)[3] or by mounting the foil specimen on a high modulus substrate which in turn is subjected to cyclic loading.[4] However, the bending/unbending (tension/compression mode) type strain-based fatigue characterization of thin specimen is more common; the investigations include the flex,[5,6] fold,[7] and roll[8] types of loading. Rather than uniform strain across the specimen, a sharp strain gradient exists from the foil surface to the approximately mid-thickness neutral surface.[9]

(Received March 1, 1999; accepted June 1, 1999)

The bending type fatigue has relevance to several real life situations in the electronic packaging. For example, the thin copper conductor line in the flexible circuit undergoes repeated strain cycling, such as for the printer hinge motion (high strain amplitude) or for the disc drive motion (low strain amplitude). The maximum strain amplitude ($\Delta\varepsilon/2$) per cycle at the conductor surface may vary from 10^{-2} (~10^1 cycles to failure) to 10^{-5} (~10^8 cycles to failure). The $\Delta\varepsilon/2$ is determined by the bend radius as well as by the line thickness (that is, by distance between the line surface and the neutral surface). The conductor line thickness may vary between several microns to about 35 μm and hence the fatigue cracks are necessarily very small; their generation at the surface and propagation through the thickness should play key roles in determining the fatigue life. In turn, the grain structure, size and anisotropy, may become critical to the passage of the fatigue crack.

In this study, we have examined the effects of grain structure, foil thickness and anneal softening on the flex fatigue of 12 to 35 μm thick rolled (R) and electrodeposited (ED) copper foils over a wide range of $\Delta\varepsilon/2$. The heavily rolled R foil corresponds to a highly pancaked anisotropic grain structure. The deposition parameters of the ED foil are manipulated to obtain a ductile foil with roughly equiaxed grain structure and about 1 μm average grain size. When prepared under optimum conditions, the ED foil has density close to that for the bulk product (such as the R foil) produced by thermomechanical processing. The ED foil, however, is saturated with the point, line and planar defects; the density of crystallographic defects increases with, among other factors, the electrodeposition overpotential.[10] This behavior is somewhat akin to that for the R foil which is characterized by a high dislocation density which, in turn, increases with the rolling reduction. Either foil type, upon thermal annealing, undergoes an attenuation of defect density, with the associated softening and often the generation of a new grain structure.[11]

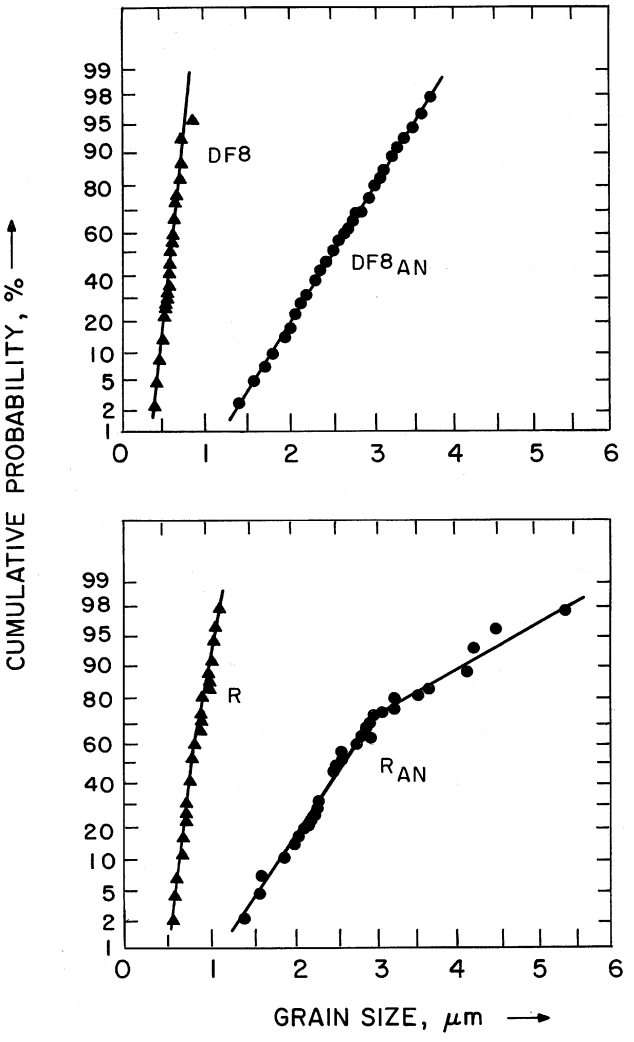

Fig. 1. Mid-thickness planar grain size distribution for the 35 μm ED (DF8) and R foils.

EXPERIMENTAL PROCEDURE

Fabrication and thermal stability of the ED and R foils have been detailed before.[11] Judicious manipulation of the deposition parameters was employed to obtain relatively smooth air side surface and to suppress a preferential z-direction grain growth or the columnar grain morphology. Using basically additive-free electrolyte, three types of ED foils were prepared: (i) at different electrodeposition overpotential levels (control foils), (ii) at optimum overpotential, circumventing localized runaway growth forms and near-substrate microporosity (DF8 foil), and (iii) at optimum overpotential to generate a stabilized grain structure relatively resistant to thermal softening (DF9 foil). The anneal softening temperature range for (i) was >100°C, for (ii) 160–180°C, and (iii) 200–220°C.

Typical cumulative distribution of grain size, characterized by the mid-thickness planar TEM, for the ED and R foils in the as-fabricated and post-anneal states, is illustrated in Fig. 1. In planar view, the grain structure was equiaxed for either foil; represented by high angle boundaries for the ED foil and by dislocation cells or subgrains of small and uneven misorientation for the R foil. The break in the cumulative distribution curve for the annealed R foil apparently corresponds to the emergence of recrystallized high angle grains. In cross section TEM, the ED foil displayed a slight z-direction extension of the grains but no evidence of columnar morphology. The large rolling reduction during fabrication of the R foil rendered its high angle as-cast or recrystallized grains severely pancaked, evident in the optical cross-section illustrated elsewhere.[12] Typically, the average size of the pancaked grain was about 0.7 μm thick (z-direction), 5–6 μm long (rolling or longitudinal direction) and 3–4 μm wide (cross-rolling or transverse direction); the thermal exposure tended to recrystallize the grain structure to some extent but the vestiges of pancaking and grain size anisotropy still remain.[11]

The flex fatigue testing procedure for thin foil has been outlined before;[13] the mandrel diameter around which the specimen flexes (bends/unbends) determines the strain amplitude ($\Delta\varepsilon/2$). The strain cycling of the 3 mm wide, 120 mm long specimen, aligned longitudinal or transverse to the cathode (ED foil) or the rolling (R foil) roll markings replicated on the foil surface, was performed at 1 Hz; using 84 g dead load to unflex the sample and to help wrap it around the mandrel. The dead load corresponds to 0.1–0.2 of the yield load. Too small dead load failed to ensure full conformity of the sample to the mandrel curvature, causing slippage and abrasion during fatigue cycling and yielding unreasonably high N_f. Too large dead load, beyond the 0.1–0.2 of the yield load, seriously reduced N_f due to an imposition of tensile stress over pure bending moment during flexing.

The fatigue life was characterized by continuous monitoring of the sample electrical resistance. The resistance change (increase) during strain cycling did

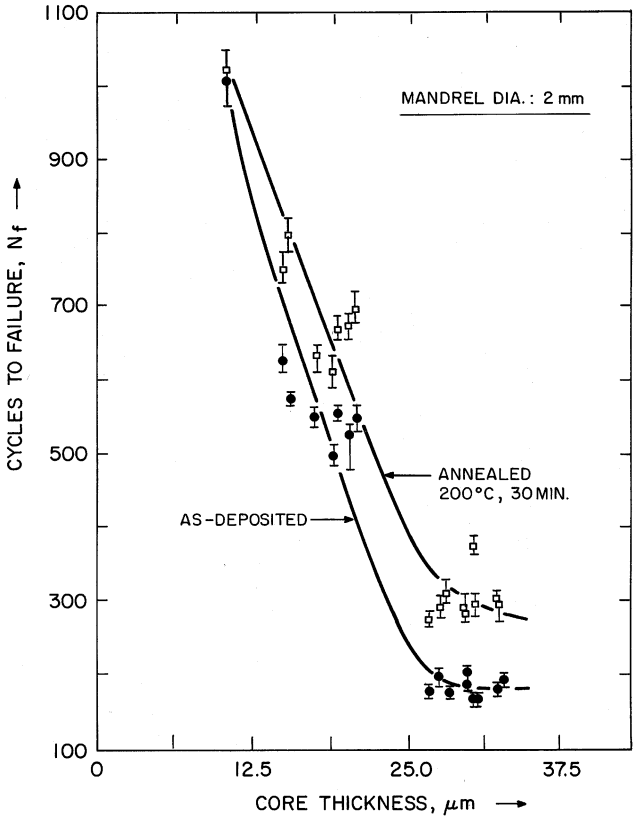

Fig. 2. Effect of core thickness and annealing on low cycle fatigue life (N_f) for the ED (DF8) foil.

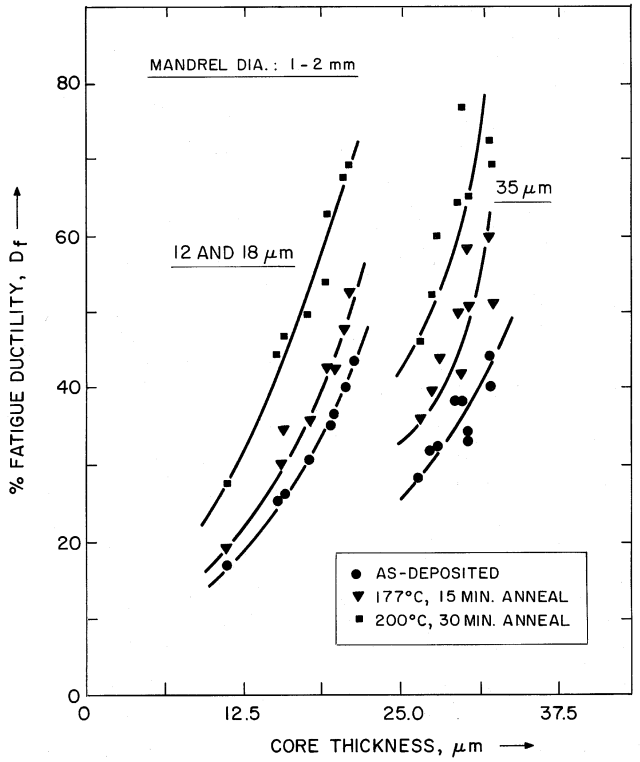

Fig. 3. Effect of core thickness on (low cycle) fatigue ductility (D_f) for the ED (DF8) foil.

not exceed a few percent, except during the terminal stages of fatigue life. At this stage, the resistance rose rapidly with the number of fatigue cycles; the failure was registered when the resistance exceeded a threshold value, typically a 100% increase, and the test was terminated for the corresponding N_f. Soon after the threshold resistance, the sample actually broke into two (infinite increase in resistance). For a given test condition, foil type and $\Delta\varepsilon/2$, three N_f observations were made and the readings averaged. The scatter between readings was less than 3% in the high $\Delta\varepsilon/2$, low N_f range but as high as 25% in the low $\Delta\varepsilon/2$, high N_f range. For selected samples, prior to the fatigue test, the sample annealing and the room temperature tensile characterization, as per the procedure outlined in our earlier paper,[14] were performed.

RESULTS

Low Cycle Fatigue

For the ED (DF8) foil, the effect of core thickness (that is foil thickness minus average air side surface profile or roughness) on N_f, using 2 mm diameter mandrel, is shown in Fig. 2. Decreasing the core thickness sharply increases N_f; by comparison, the enhancing effect of 200°C, 30 minute anneal on N_f is small. Using the iterative calculation procedure,[5] for the mandrel diameters between 1 and 2 mm, the fatigue ductility parameter D_f (see Appendix, Eq. 1) was determined for the as-deposited and annealed 177°C, 15 minutes and 200°C, 30 minutes) DF8 foils;

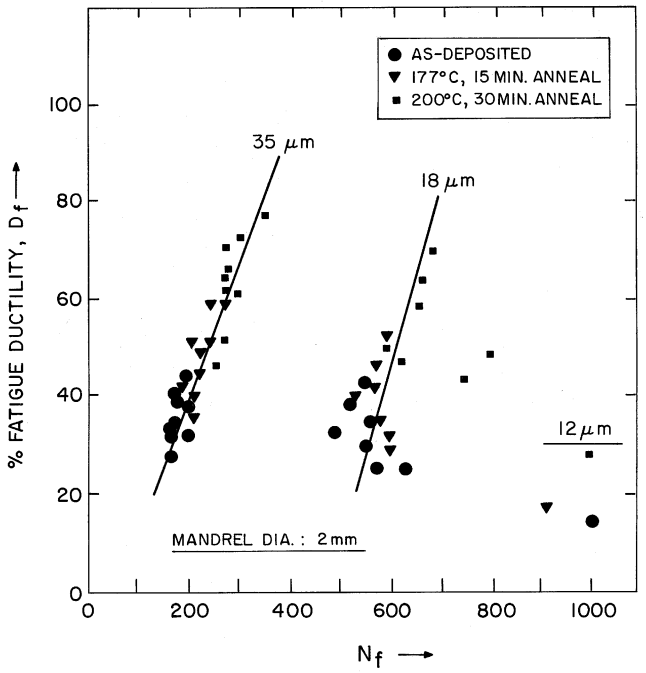

Fig. 4. Relationship between D_f and N_f for the ED (DF8) foil.

the results are shown in Fig. 3. Here the parameter D_f is a measure of strain accommodation (during low cycle fatigue) prior to failure;[6] it should be independent of $\Delta\varepsilon/2$ determined by mandrel diameter and foil thickness. However, increasing the core thickness for a given average foil thickness (that is, decreasing the surface profile or roughness) and increasing the anneal

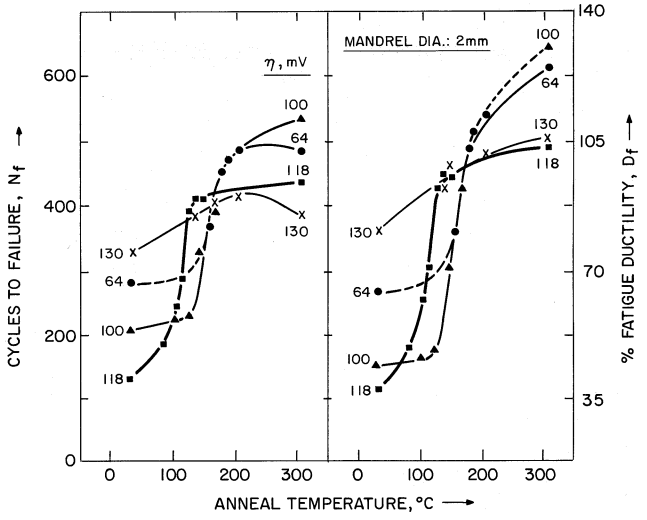

Fig. 5. Effect of electrodeposition overpotential (η) on N_f and D_f in terms of (30 min) anneal response, for the 35 μm ED control foil.

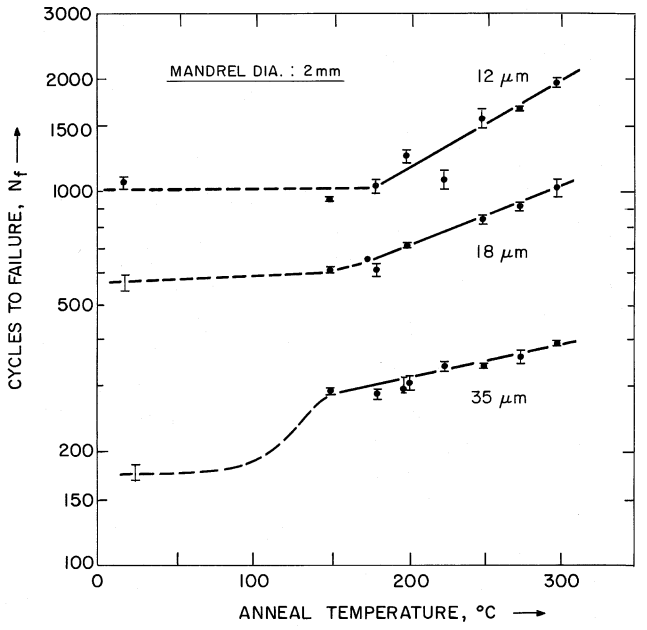

Fig. 6. Effect of foil thickness on (30 min) anneal response of N_f for the ED (DF8) foil.

temperature enhance D_f. For a given foil thickness, the annealing enhances N_f as well as D_f, as shown in Fig. 4 for fatigue cycling around 2 mm diameter mandrel; the anneal induced enhancement of D_f proceeds along a straight line, the lowest data points represent the as-deposited state and the highest data points the effect of maximum anneal temperature (300°C). Here the scatter is apparently related to variations of the air side surface profile or roughness.

The anneal response of the ED foil depends, among other factors, upon the electrodeposition overpotential (η).[11] The anneal induced enhancement of N_f and D_f, likewise, depends upon η as shown in Fig. 5 for the 35 μm control foil in low cycle fatigue employing 2 mm diameter mandrel. An optimum η (100 mV) maximizes the anneal response[11] as well as the enhancement of N_f and D_f. Under this condition, (i) a marked N_f and D_f

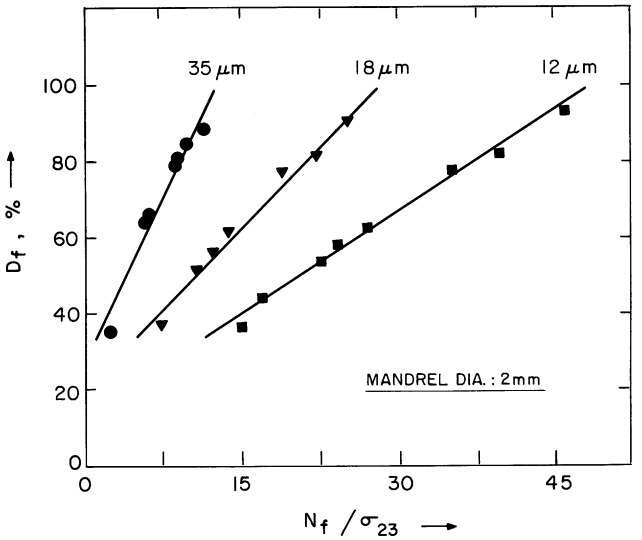

Fig. 7. Effect of foil thickness and strength (σ) normalized fatigue life (N_f/σ) on fatigue ductility (D_f) for the ED (DF8) foil.

response within a narrow range of anneal temperatures and (ii) about three-fold increase in the fatigue performance after 300°C, 30 minutes anneal are indicated. Note sharp increases of N_f and D_f around 100°C (η ≈ 118 mV) and 150°C (η = 64–100 mV), clearly related to the anneal-induced recrystallization-like microstructural changes.[15] For the 12, 18, and 35 μm thick ED (DF8) foils electro-deposited at η_{opt}, the effect of anneal temperature on N_f (using 2 mm diameter mandrel) is shown in Fig. 6 on a semi-logarithmic scale. The break in curves between 150 and 180°C is again indicative of the microstructural modification.

A good fit for the D_f versus N_f plot (compare Fig. 4) is obtained when N_f is normalized with respect to the room temperature (23°C) tensile strength (σ_{23}), as illustrated in Fig. 7 for the 12, 18, and 35 μm ED (DF8) foils. Whereas N_f is sensitive to the geometrical parameters (foil thickness and mandrel diameter), D_f is implicitly independent of these factors. Hence for a given change in D_f, the thinner foil generates much larger changes in N_f/σ_{23}. In fact, the D_f versus N_f/σ_{23} plot for a given foil thickness (or Δε/2) has an universal character[6] whereby a variety of ED and R foils follow an identical path upon annealing. This is illustrated in Fig. 8 for the 35 μm ED (DF8) and R foils in the as-fabricated and annealed conditions. Here the lowermost regions of the universal curve correspond to the as-fabricated R foil; further up the curve to the as-deposited ED foil. The effect of annealing is to move upwards along the curve, increasing N_f/σ_{23} and D_f, the efficacy of annealing determining the exact location on the curve.

Coffin-Manson Representation

For the as-fabricated and annealed (225°C, 10 minutes) 18 μm ED (DF8) and R foils, the Coffin-Manson (C-M) logarithmic plots are shown in Figs. 9 ($2N_f = 10^2$ to 10^5) and 10 ($2N_f = 10^4$ to 5×10^6). The longitudinally (L) oriented samples show higher N_f

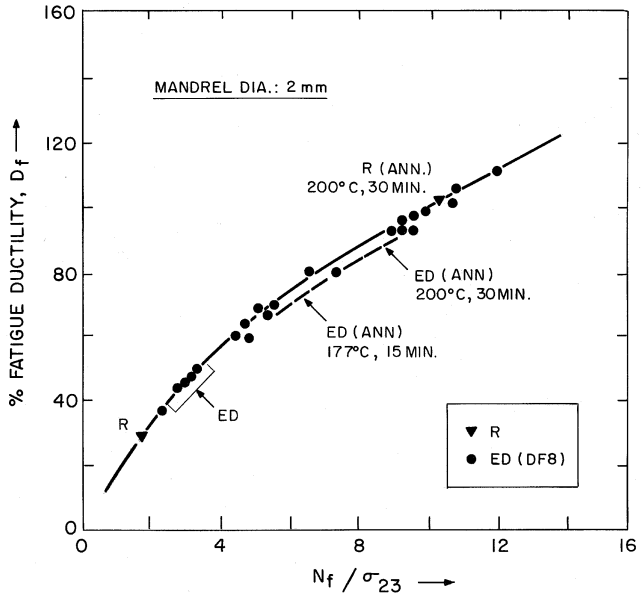

Fig. 8. Universal relationship between D_f and N_f/σ for the 35 μm ED (DF8) and R foils.

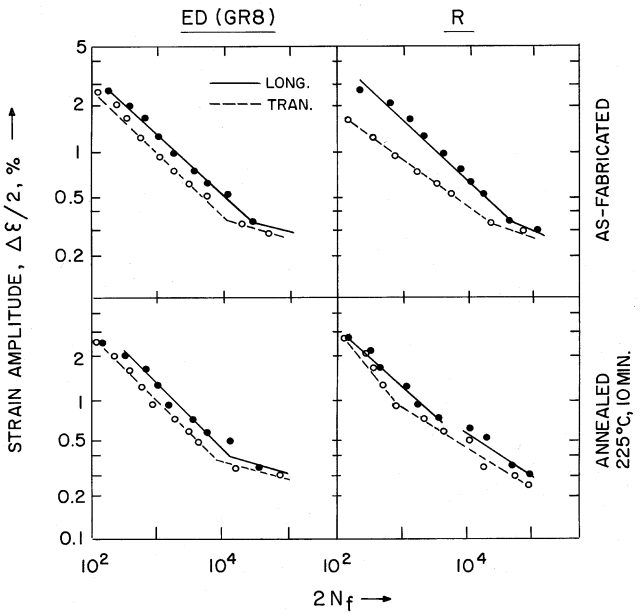

Fig. 9. Coffin-Manson representation for the 18 μm ED (DF8) and R foils showing the plastic to elastic transition in fatigue response.

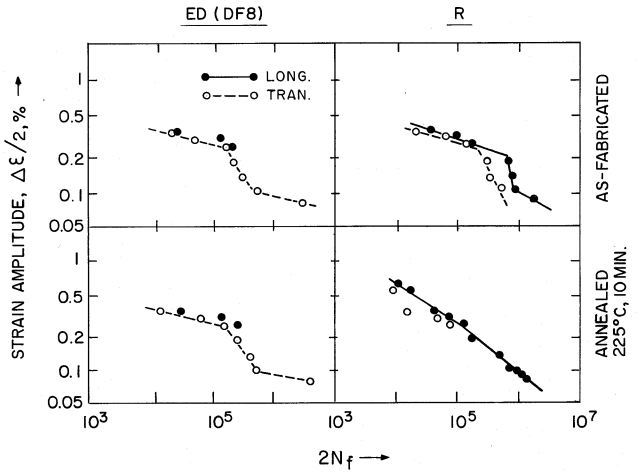

Fig. 10. Coffin-Manson representation for the 18 μm ED (DF8) and R foils in high cycle flex fatigue.

than do the transversely (T) oriented samples, the directional anisotropy is particularly large for the as-fabricated R foil. The transition from the plastic (low cycle) to the elastic (high cycle) cyclic response occurs at (N_t) about 10^4 cycles to failure (Fig. 9); N_t for the L orientation is somewhat greater than that for the T orientation. The C-M slopes c and b in the low and the high cycle fatigue respectively (see Appendix, Eq. 2), as expected, are close to 0.5 and 0.1 in the plastic and elastic regimes respectively (Table I). The abnormal N_t and c values for the R foil are apparently due to hydrogen embrittlement typical for the ETP copper.[16] Except for the annealed R foil, the high cycle C-M plots (Fig. 10) show an intermittent increase of slope, as has been observed and explained by Pederson.[17]

The fatigue ductility parameter D_f, ascertained from the low cycle data by iteration,[5] is directly related to the intercept ε_f' at $2N_f = 1$ (Eq. 1a) or to the true strain at fracture (ε_f) (Eq. 3a). It is possible to calculate the C-M slope c in the low cycle regime utilizing N_f (Eq. 1b); likewise, starting with N_f in the high cycle regime and D_f, the C-M slope b in the high cycle regime may be calculated (Eq. 1c). Utilizing b and c, the parameters K′ (Eq. 4a) and n′ (Eq. 4b–d) of the stress-strain curve in cyclic loading are ascertained. Table I illustrates the calculated values of D_f, b, and n′; the cyclic strain hardening parameter n′ is compared

Table I. Fatigue Parameters for 18 μm Ed and R Foils

	ED (DF8)		R-T⁺		R-L⁺⁺	
	AF⁺⁺	ANN⁺⁺⁺	AF⁺⁺	ANN⁺⁺⁺	AF⁺⁺	ANN⁺⁺⁺
–c (exp)	0.43	0.43	0.38	0.56	0.46	0.44
D_f (calc)	0.42	0.50	0.22	0.50	0.82	0.68
–b (calc)	0.12	.012	0.12	0.09	—	—
n (exp) – Tensile	0.20	0.17	0.26	0.15	—	—
n′ (calc) – Cyclic	0.27	0.27	0.33	0.16	—	—

⁺Orientation: T = traverse, L = longitudinal to rolling direction
⁺⁺As fabricated: ED = electrodeposited, R = as rolled
⁺⁺⁺Annealed: 200–225°C, 15–20 min

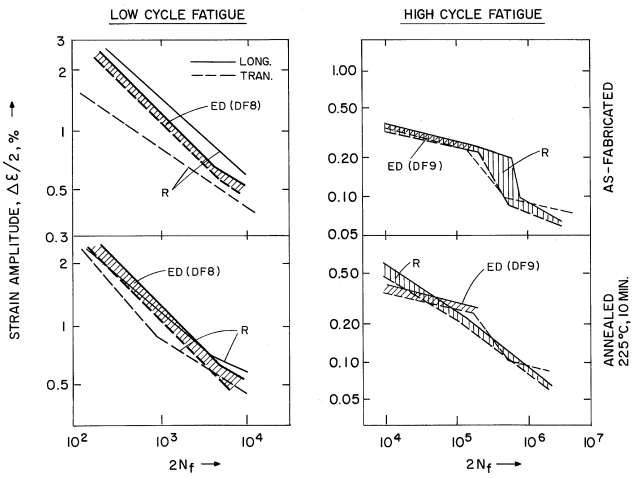

Fig. 11. Comparison of cyclic response of the 18 μm ED and R foils in the high and low Δε/2 fatigue regimes.

with the corresponding parameter n determined experimentally in the monotonic loading. Note a large directional anisotropy of c (experimental) and D_f for the R foil due to grain pancaking caused by severe rolling reduction. The anneal induced softening generally results in an enhancement of D_f; except for the R foil in L orientation, perhaps due to the embrittlement effects. For the T orientation R foil, annealing causes significant reduction of b, n, and n′. Since n′ is consistently higher than n, a higher strain hardening rate in the cyclic (than in the monotonic) loading is indicated. Note that with increasing n′, both c and b decrease (Eqs. 4b and 4c), the effect is greater on c (Eq. 4d); hence N_f in the low as well as the high cycle fatigue is enhanced for a high n′ foil.

Crack Propagation

A comparison of the 18 μm ED and R foils in the low and the high cycle fatigue is shown in Fig. 11, omitting the data points for clarity of presentation. For the ED foil, DF8 has been employed in the low cycle fatigue; DF9, due to its greater microstructural stability in cyclic loading, has been employed in the high cycle fatigue. The R foil is prone to considerable directional anisotropy due apparently to grain pancaking; the anisotropy, however, decreases with annealing, which tends to erase the pancaked grain structure, and with decreasing Δε/2. Note a greater tendency of the ED foils (than of the R foil) to form a knee at N_t (DF8) and an intermittent increase of the C-M slope (DF9) in the high cycle fatigue. The R foil in L orientation displays distinctly superior N_f over much of the Δε/2 range; following the 225°C, 10 minute anneal, however, the ED (DF8) foil offers somewhat better resistance in the low cycle fatigue. The post-anneal high cycle fatigue performance of the R and ED (DF9) foils is roughly identical.

A careful investigation of initiation and propagation of fatigue cracks has revealed that[18]

i. cracks initiate at the foil surface where Δε/2 is maximum

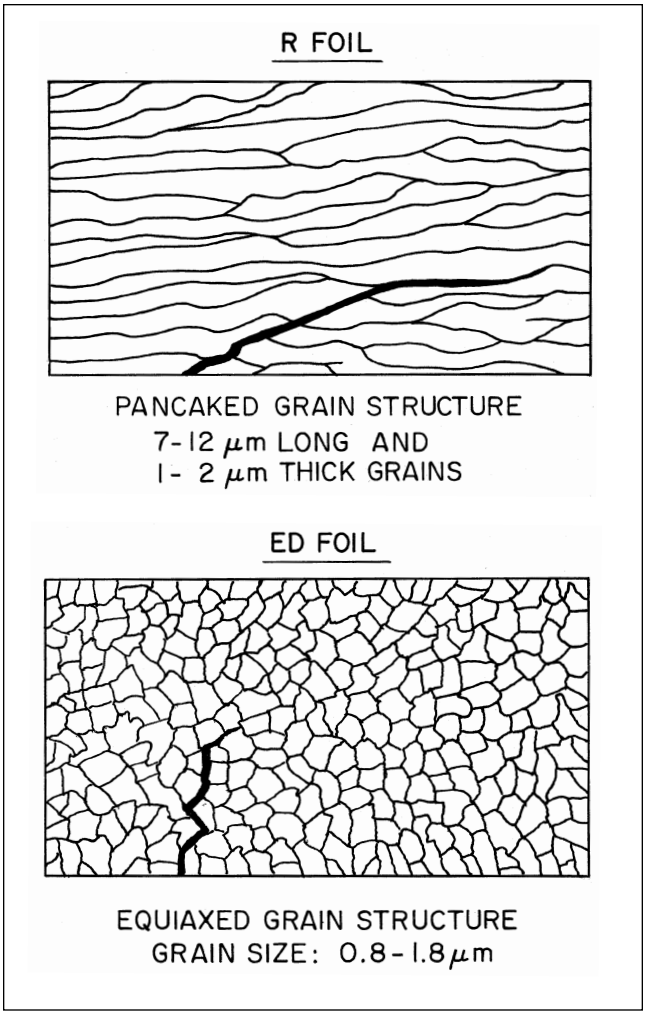

Fig. 12. Schematic of the through-thickness intergranular propagation of fatigue crack for the R and ED foils.

ii. cracks propagate along the high angle grain boundaries across width and through thickness of the sample
iii. in the low cycle fatigue, numerous cracks initiate early during fatigue life (that is, at $N/N_f \gtrsim 0$); most of these cracks remain stationary, appearing as surface notches in cross-section, but a small fraction moves inward from the surface (into the lower Δε/2 regime) with increasing number of cycles
iv. in the high cycle fatigue, the crack initiation is difficult; only a few cracks (often a single crack) nucleate at $N/N_f \lesssim 1$ and soon after propagate rapidly
v. high angle grain boundaries oblique to the crack propagation direction (as for the R foil) hinder the forward motion of the crack
vi. a single crack propagating simultaneously across the 3 mm sample width and through the 12 to 35 μm sample thickness becomes the fatal crack corresponding to N_f.

Based on numerous microscopic observations,[18] a schematic of crack propagation in transverse cross-section, for the ED and R foils, is shown in Fig. 12. Note the width-wise drift of fatigue crack for the R foil

whereas the crack moves straight across foil thickness for the ED foil. A finer grain structure or a more severe pancaking should provide a greater resistance to crack propagation. Since the equiaxed grain size (ED foil) and the thickness of pancaked grains on the average are approximately the same, it is not surprising that the fatigue response of the two foil types is similar (Fig. 11); except that the R foil in T orientation in the low cycle fatigue shows distinctly inferior N_f over a wide range of $\Delta\varepsilon/2$.

Metallurgical Effects

The (mid-thickness planar) grain size distribution of the annealed (225°C, 10 min.) 18 μm ED (DF8) and R foils is shown in Fig. 13. For the R foil, the "grain" corresponds to the post-anneal dislocation cell which appears as an equiaxed grain with somewhat diffuse boundaries. The pancaked grain with high angle boundaries is slightly larger (than the subgrain) in the thickness direction but is considerably larger (several microns) in the length (rolling) and the width (cross-rolling) directions. The effect of cyclic loading is to deplete the grain interior of dislocation features and to further sharpen the grain boundaries. Figure 14 shows the effect of cyclic loading at $\Delta\varepsilon/2 = 0.5\%$ on the cumulative grain size distribution (the dotted line represents the pre-fatigue distribution). For the R foil, no measurable effect of fatigue on grain size is observed. However for the ED foil, a small but significant shift in distribution, indicating a grain size reduction, occurs; apparently, the dislocation features in some of the larger grains upon fatigue form the new smaller grains.

Figure 15 shows the effect of cyclic loading ($\Delta\varepsilon/2 = 0.5\%$) on the average electrical resistance and on the average softening (a reduction in mid-thickness microhardness) of the 35 μm foil. The resistance increases with N/N_f, indicative of fatigue induced damage; the effect is greater for the ED foil (than for the R foil). The resistance increase up to $N/N_f = 0.87$ is less than 2% but as N/N_f approaches unity accelerating resistance is indicated; the fatal failure is registered when the resistance increase is in excess of 100%. In spite of prior anneal softening, considerable further softening occurs upon cyclic loading; the effect is again greater for the ED foil. The fatigue induced softening, apparently due to strain localization, was highly uneven, as has been observed before for the electrodeposited copper foil[19] and for the annealed polycrystalline copper.[20]

Table II summarizes softening in the low cycle and the high cycle fatigue for the as-fabricated and the annealed (191°C, 15 min.) 18 μm ED (DF8) and R foils, averaged over $N/N_f = 0.5$, 0.75, and 0.875, in the L and T orientations. The softening is greater in the high cycle fatigue; and in the annealed state for the ED foil and in the as-fabricated state for the R foil. The as-fabricated R foil tends to soften; however, the annealed R foil in the low cycle fatigue tends to harden on the average. The reversal of average softening in Fig. 15 is perhaps suggestive of the simultaneous softening

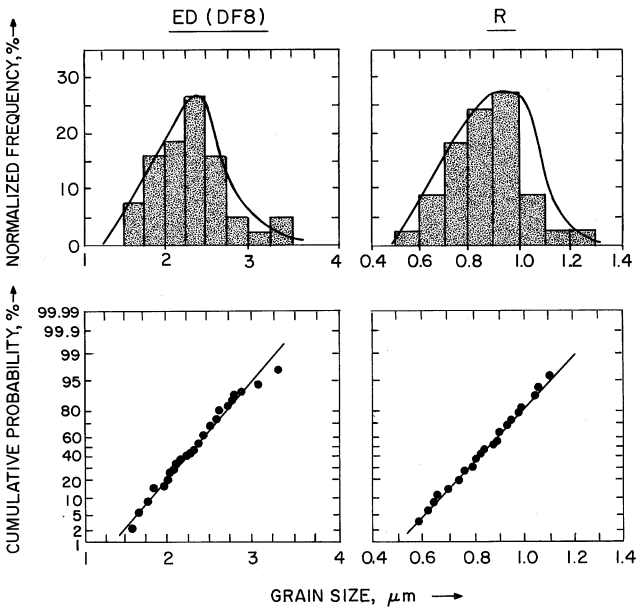

Fig. 13. Typical (planar mid-thickness) grain size distribution for the 18 μm ED (DF8) and R foils prior to flex fatigue (225°C, 10 min anneal).

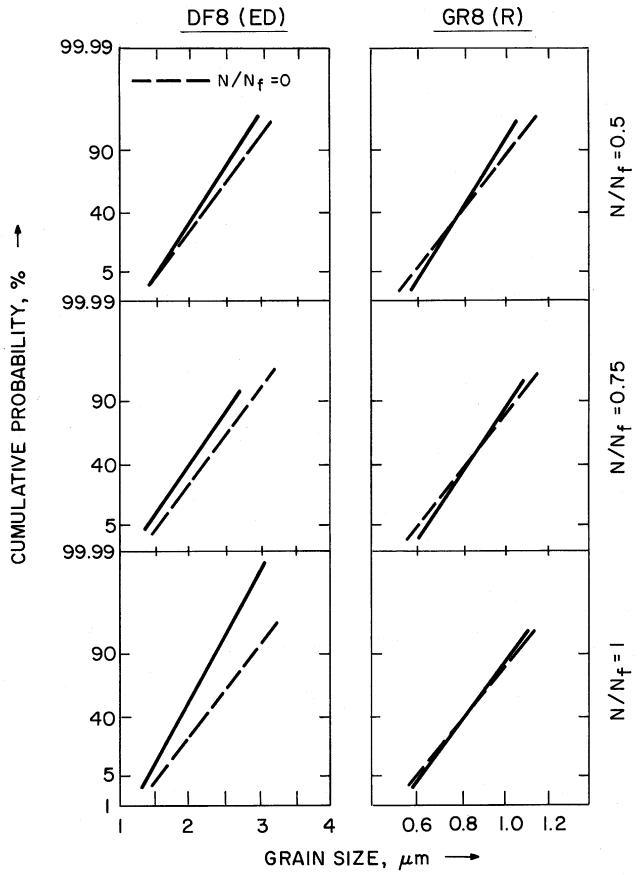

Fig. 14. Variation in (planar mid-thickness) grain size cumulative distribution with flex fatigue (18μm foil; 225°C, 10 min anneal).

and hardening processes at work for both the R and ED foils as N/N_f approaches unity. As a general rule, when $n > 0.15$ or σ/σ_y (σ_y is yield strength and σ is ultimate strength) >1.4, cyclic hardening is predicted; when $n < 0.15$ or $\sigma/\sigma_y < 1.2$, cyclic softening may

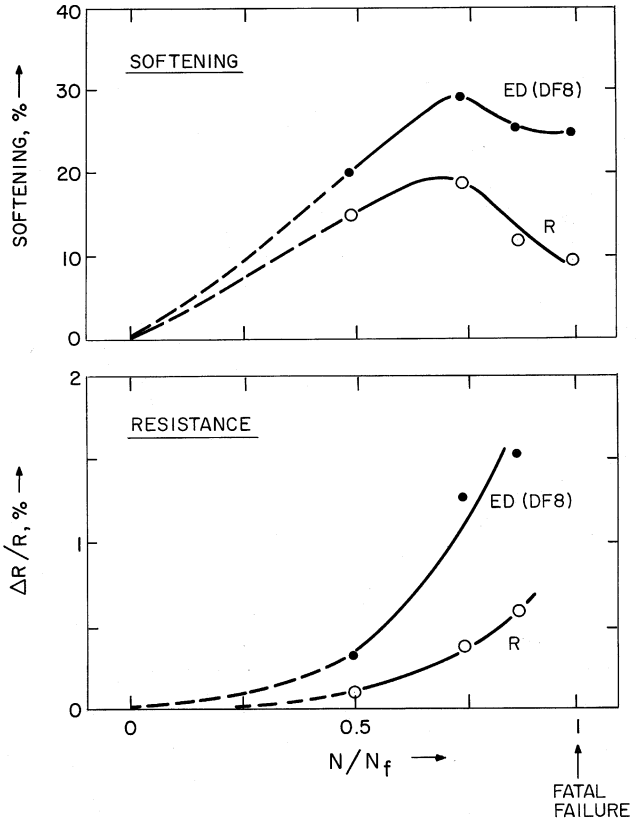

Fig. 15. Effect of flex fatigue on softening and electrical resistance for the annealed 35 μm foil.

occur.[21] For the R foil, the calculated n′ (see Table I) pre-anneal is 0.33 but after dead-soft (225°C, 10 min.) anneal it becomes 0.14. Accordingly, the pre-anneal R foil (a material with relatively high stacking fault energy) is prone to soften during fatigue but in the post-anneal condition should show considerable cyclic hardening.[22] For the ED foil, the n′ in the pre-anneal and post-anneal states remains identical (0.27) and softening during cyclic loading is anticipated.

The predominant post-fatigue microstructure in the planar and the cross-section microscopy was featureless micron-sized grains bounded by sharp boundaries. The shear bands[23] or persistent slip bands were only sporadically observed. The dislocation configurations, encountered[1,24] after stress-control cyclic loading for the large grain (secondary recrystallization, 200 μm) thin rolled and annealed foil, or observed[25] or predicted[17] for the relatively large grain bulk polycrystalline copper in strain-based fatigue, were rarely found in our experiments. Small grain size and proximity of the surface are perhaps responsible for this. The dislocation patterning in fatigue is prohibited for the sub-micron grain structure; when the grain size approaches 1 μm, the formation of dislocation grids overlaying grain boundaries can be favored.[26] We found some evidence of banding, patterning and grid formation halfway between the sample surface and the center (mid-thickness) by off-center planar TEM, as illustrated in Fig. 16. Bulk of the microstructure, however, is equiaxed high angle grains, occasionally traversed by twins.

CONCLUDING REMARKS

The Coffin-Manson parameters c (low cycle fatigue), b (high cycle fatigue), D_f, N_f, and n′ in flex (bending/unbending) fatigue for the thin copper foil are more or less the same as in strain controlled fatigue for the larger scaled polycrystalline copper. In the absence of embrittlement effects, thermal annealing should decrease b, c and increase D_f, n′; effectively enhancing N_f. The efficacy of annealing in increasing N_f depends upon the thermal modification of the foil microstructure. An optimally prepared (rolling reduction or deposition overpotential) and annealed smooth foil of minimum thickness yields high N_f and D_f. For a given foil thickness, D_f versus N_f/σ plot describes an universal anneal response of the copper foil.

The cyclic loading results in simultaneous hardening (n′) and non-uniform softening (drop in microhardness). However, the associated dislocation patterning, characteristic of the strain localization, is difficult to observe by microscopy due to the close proximity of the grain boundaries (fine grain structure) and of the sample surface (very thin foil). For the ED foil, as-deposited or annealed, the net effect of cyclic loading is significant softening. For the R foil, the as-fabricated (initially hard) foil softens but the anneal softened foil hardens during fatigue.

The fatigue cracks initiate on the sample surface and propagate along the grain boundaries across the sample width and through its thickness. The fine equiaxed grain structure provides a tortuous crack propagation path whereas the grain boundary oblique

Table II. % Softening Due to Fatigue Cycling for the ED and R Foils

$\Delta\varepsilon/2$, % →	2.50 (Low Cycle)				0.18 (High Cycle)			
	Average⁺		Maximum		Average⁺		Maximum	
Foil →	AF⁺⁺	ANN⁺⁺	AF⁺⁺	ANN⁺⁺	AF⁺⁺	ANN⁺⁺	AF⁺⁺	ANN⁺⁺
ED (DF8)	16	20	21	25	20	28	25	39
R	15	–3	17	16	24	16	35	25

⁺ average between N/N_f = 0.5, 0.75, 0.875 in L and T orientations
⁺⁺ AF = as fabricate, ANN = annealed 191°C, 15 min

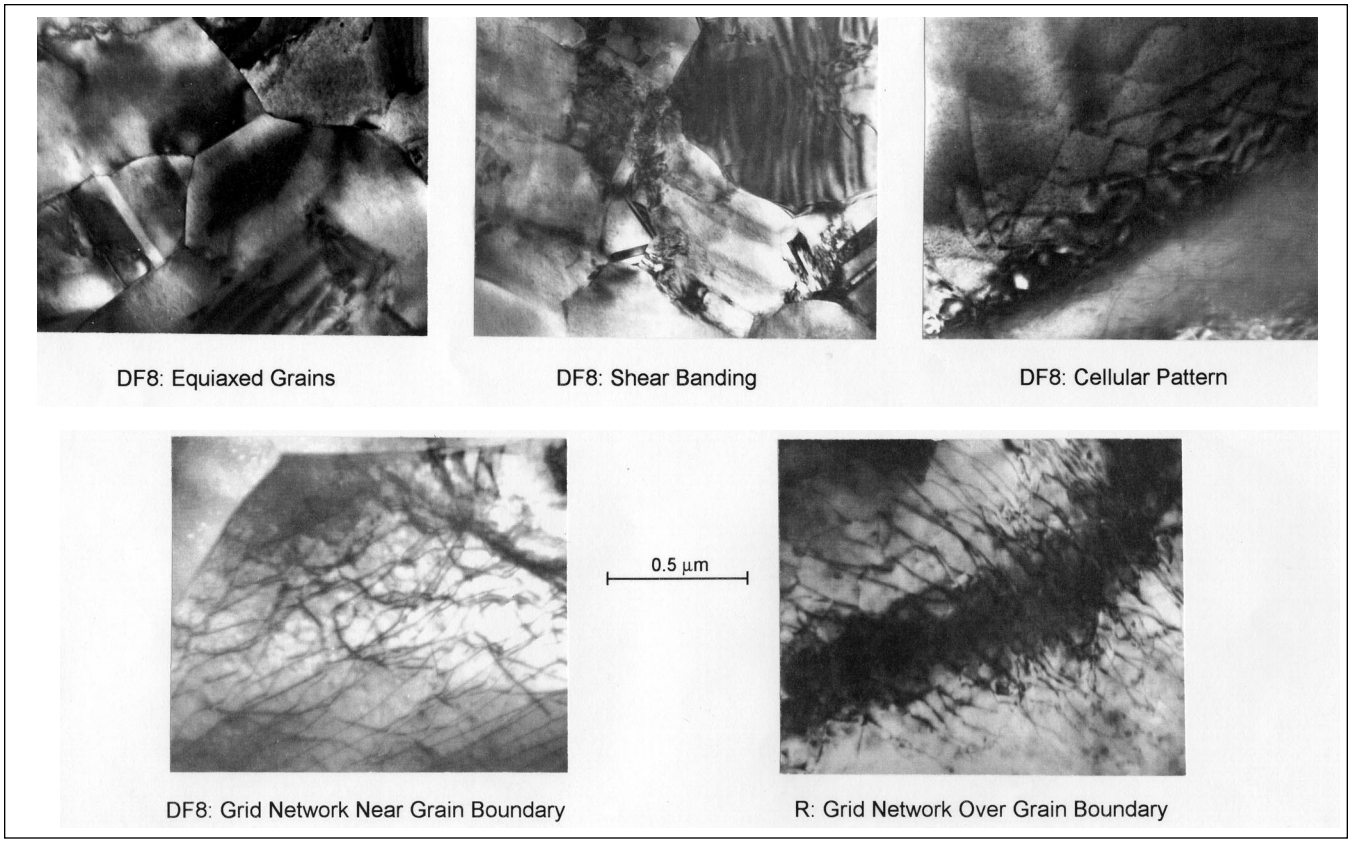

Fig. 16. Grain structure and dislocation configurations in planar TEM halfway between mid-thickness and foil surface (18μm annealed foil, $N/N_f = 1$).

to the crack path, as for the pancaked grain structure of the R foil, presents an effective obstruction to crack propagation; compelling a width-wise drift of the fatigue crack. The fatal crack ($N = N_f$) corresponds to an asymptotic increase of the electrical resistance (which rises only modestly for $N < N_f$).

The grain pancaking due to heavy rolling for the R foil renders N_f higher in the L (than in the T) orientation. In the annealed state and for the high cycle fatigue, N_f for the ED (fine equiaxed grain structure) and R (fine equiaxed grains sandwiched between the boundaries of the pancaked grains) foils is identical over a wide range of $\Delta\varepsilon/2$. However, in the low cycle fatigue, the unique crack propagation habit of each foil type, as-fabricated or annealed, tends to differentiate N_f for the ED and R foils.

REFERENCES

1. M. Judelewicz, *Scripta Metall. Mater.* 29, 1463 (1993).
2. S. Hong and R. Weil, *Thin Solid Films* 283, 175 (1996).
3. H. Hayashi, S. Nishikawa, and K. Nitta, *Printed Circuit World Convention IV* (Northbrook, IL: Institute for Interconnecting and Packaging Electronic Circuits, 1987).
4. Y. Nagase and T. Yoshizake, *JSME Inter. J.*, Ser. 1, 34, 56 (1991); *Exp. Mech.* 33, 49 (1993).
5. W. Engelmaier and A. Wagner, *Circuit World* 14, 30 (1988).
6. H.D. Merchant, M.G. Minor, S.J. Clouser, and D.T. Leonard, *Circuit World* 25, 38 (1998).
7. H.D. Merchant, S.J. Clouser, and M.G. Minor, *FLEXCON'96* (Neffs, PA: Semiconductor Technology Center, 1990).
8. R. Watanabe, N. Ohya, K. Sugaya, Y. Nagai, and S. Sakai, *Copper '90* (London, UK: Inst. Mets, 1990), p. 535.
9. N.E. Dowling, *J. Eng. Materials Tech.* 100, 157 (1978).
10. H.D. Merchant and D.B. Girin, *Electrochemical Synthesis and Modification of Materials,* MRS Proc. 431 (Pittsburgh, PA: MRS, 1997), p. 433.
11. H.D. Merchant and M.G. Minor, Jr.,*Thermal Softening of Thin Copper Foil* (submitted for publication).
12. H.D. Merchant and S.J. Clouser, *IPC National Conference, Flex Circuits* (Northbrook, IL: Institute for Interconnecting and Packaging Electronic Circuits, 1996).
13. The flex fatigue tests were performed as per the ASTM ET-86a and E345 guidelines.
14. H.D. Merchant, *J. Electron. Mater.* 22, 631 (1993).
15. H.D. Merchant, *J. Electron. Mater.* 24, 919 (1995).
16. L.S. Kotova and V.M. Rozenberg, *Phys. Met. Metall.* 35, 181 (1973).
17. O.B. Pedersen, *Acta Metall. Mater.* 38, 1221 (1990).
18. "Fatigue Damage Characterization in Copper Foil and Copper/Polyimide Constructions" (to be published in *J. Electron. Packaging*).
19. Y. Nagase and T. Yoshizaki, *JSME Inter. J.* (Ser. 1) 34, 56 (1991).
20. J. Polak, K. Obrtlik, M. Hajek, and A. Vasek, *Mater. Sci. Eng.* A151, 19 (1992); A154, L15 (1992).
21. S.S. Manson and M.H. Hirschberg, *Fatigue: An Interdisciplinary Approach* (Syracuse, NY: Syracuse University Press, 1964), p.133.
22. C.E. Feltner and C. Laird, *Acta Met.* 15, 1621 (1967).
23. S.R. Agnew, A.Yu. Vinogradov, S. Hashimoto, and J.R. Weertman, *J. Electron. Mater.* this issue.
24. M. Judelewicz, H.U. Kunzi, N. Merk, and B. Ilschner, *Mat. Sci. Eng.* A186, 135 (1994).
25. J.C. Figueroa, S.P. Bhat, R. De La Veaux, S. Murzenski, and C. Laird, *Acta Metall.* 29, 1667 (1981).
26. M.V. Glazov and C. Laird, *Acta Metall. Mater.* 43, 2849 (1995).

APPENDIX

Three well known empirical relations[a–c] describe the strain controlled fatigue:

$$\frac{\Delta\varepsilon}{2} = D_f^{0.75} N_f^{-0.6} + 0.9\left(\frac{\sigma}{E}\right)\left[\exp(D_f)/0.36\right]^{0.1785(10^5/N_f)} \quad (1)$$

$$\frac{\Delta\varepsilon}{2} = \varepsilon_f'(2N_f)^c + \frac{\sigma_f'}{E}(2N_f)^b \quad (2)$$

$$\Delta\varepsilon = \varepsilon_f^{0.6}\, N_f^{-0.6} + 3.5\,(\sigma/E)\, N_f^{-0.12} \quad (3)$$

where N_f is fatigue life, $\Delta\varepsilon/2$ strain amplitude, D_f fatigue ductility parameter, σ tensile strength, ε_f true strain at fracture and E Young's modulus; the first term in each equation describes the plastic response in low cycle fatigue and the second term the elastic response in high cycle fatigue.[d] Equating the first and second terms respectively of Eqs. 1 and 2, it follows that

$$D_f = (\varepsilon'_f)^{1.33} \quad (1a)$$

$$c = -0.6 \log(N_f)/\log(2N_f) \quad (1b)$$

$$b \approx -[\log(2N_f)]^{-1}\,[1.29 + \log(e^{D_f}) - 0.1785 \log N_f) \quad (1c)$$

Likewise, equating the first term of Eqs. 1 and 3,

$$D_f \approx \varepsilon_f^{0.8} \quad (3a)$$

The stress-strain curve in cyclic loading, adding the plastic and elastic components, is described by[e]

$$\Delta\varepsilon = (\Delta\sigma/K')^{1/n'} + \Delta\sigma/E \quad (4)$$

where

$$K' = \sigma_f'/(\varepsilon_f')^{n'} \quad (4a)$$

σ_f' and ε_f', the parameters in Eq. 2, are the intercepts of the elastic and plastic components respectively at $2N_f - 1$ and n' is the strain hardening parameter in cyclic loading, related to the slopes c and b in Eq. 2 as[e]

$$b = -n'/(1+5n') \quad (4b)$$

$$c = -1/(1+5n') \quad (4c)$$

$$b/c = n' \quad (4d)$$

REFERENCES

a. W. Engelmaier and A. Wagner, *Circuit World* 14, 30 (1988).
b. T.H. Courtney, *Mechanical Behavior of Materials* (New York: McGraw-Hill, 1990), p. 562.
c. M.A. Meyers and K.K. Chawla, *Mechanical Metallurgy: Principles and Applications* (Englewood Cliffs, NJ: Prentice-Hall, 1984), p, 688.
d. N.E. Dowling, *Mechanical Behavior of Materials* (Englewood Cliffs, NJ: Prentice-Hall, 1993), p. 621.
e. J.D. Morrow, "Internal Friction, Damping and Cyclic Plasticity," ASTM STP 378 (Philadelphia, PA: ASTM, 196), p. 72.